



On the role of water in selective hydrogenation of cinnamaldehyde to cinnamyl alcohol on PtFe catalysts



Yihu Dai^{a,*}, Xing Gao^a, Xiaofang Chu^a, Chunyang Jiang^a, Yao Yao^a, Zhen Guo^a, Chunmei Zhou^a, Chuan Wang^a, Hongming Wang^{b,*}, Yanhui Yang^{a,*}

^a Institute of Advanced Synthesis (IAS), School of Chemistry and Molecular Engineering, Jiangsu National Synergetic Innovation Center for Advanced Materials, Nanjing Tech University, 211816 Nanjing, China

^b Institute of Advanced Study and College of Chemistry, Nanchang University, 330031 Nanchang, China

ARTICLE INFO

Article history:

Received 24 March 2018

Revised 6 May 2018

Accepted 7 May 2018

Keywords:

Water

Selective hydrogenation

α,β -Unsaturated aldehyde and alcohol

Bimetallic catalyst

Hydrogen exchange

ABSTRACT

A series of carbon nanotube (CNT)-supported bimetallic PtFe nanoparticles were synthesized and employed as catalysts for hydrogenation of cinnamaldehyde in pure water. A synergy between water and bimetallic PtFe catalysts has allowed the efficiently selective production of cinnamyl alcohol. With the aid of water, an initial reaction rate of $>1200\text{ h}^{-1}$ and a high selectivity of $>97\%$, as well as a good cycling stability, were achieved with a Pt₃Fe/CNT catalyst under mild reaction conditions. Isotopic labeling studies and theoretic calculation results demonstrated that the water-involved hydrogen-exchange pathway occurred with a lower energy barrier, which coexisted with the pathway of direct H₂ dissociation–hydrogenation. This work also suggested that water participated in the catalytic hydrogenation reaction by serving as a hydrogen-exchange bridge.

© 2018 Elsevier Inc. All rights reserved.

1. Introduction

The chemoselective hydrogenation of carbonyls in multiunsaturated hydrocarbons, particularly α,β -unsaturated aldehydes and ketones, is a longstanding challenge, since both thermodynamics and kinetics favor the hydrogenation of C=C bonds over C=O bonds [1]. A variety of heterogeneous metallic catalysts have been developed to control the selectivity of the reaction by means of alloying, ligand modification, and support optimization [2–10]. The elucidation of geometric and electronic effects on Pt-catalyzed hydrogenation reactions has been attempted. The selectivity of C=O hydrogenation exhibits a strong dependence on the particle size distribution, and the reaction rate is also sensitive to the structure of the Pt nanoparticles [11–13]. The electronic modification of Pt in bimetallic catalysis is an effective strategy for improving catalytic performance. However, the lack of structural control limits further enhancement because the second metal promoter unselectively blocks the Pt active sites. Surface science studies have suggested that direct adsorption of substances on the self-assembled layers of ligands is critical to adjusting the selectivity of the hydrogenation. The arrangement and the

orientation of ligands with different chain lengths on the metal surfaces can be used to tune the adsorption geometry of the aldehyde molecule and boost the hydrogenation selectivity [14]. The confinement of metallic Pt or Pd sites in porous metal–organic frameworks also promotes the selectivity of the C=O activation due to steric hindrance of the C=C group as it approaches the active sites [15–17]. In addition, the catalytic performance depends on the manipulation of kinetic parameters (e.g., temperature, pressure, and humidity).

The use of water as a promoter or inhibitor to enhance the activity and selectivity of a catalyst has been demonstrated in many types of reactions, including CO oxidation, methanation, Fischer–Tropsch synthesis, oxygen evolution reactions, and various processes used in organic synthesis [18–23]. The extensive interest in the utilization of water is due to its substantial economic and ecological advantages, as well as its various functions, including solvation effects, carbon removal, and surface reconstruction [24–27]. A reaction pathway followed by a water-mediated Mars–Van Krevelen reaction has been reported in single-atom Pt₁/CeO₂-catalyzed CO oxidation. The intermediate is formed via the interaction of CO and the hydroxyl group from the dissociation of water rather than the direct reaction of CO with the lattice oxygen [28]. The Au-catalyzed oxidation of CO has also been enhanced by water-promoted decomposition and conversion of the reaction intermediates [29]. Recently, water-assisted hydrogen diffusion

* Corresponding author.

E-mail addresses: ias_yhdai@njtech.edu.cn (Y. Dai), hongmingwang@ncu.edu.cn (H. Wang), yhyang@njtech.edu.cn (Y. Yang).

across the surface of a metal oxide was directly confirmed by scanning tunneling microscopy (STM) movies, suggesting that catalytic hydrogenation, hydrogen evolution, or the reformation of hydrogen may be accelerated by the presence of water [30]. For instance, it was found that water could take part in the synthesis of C_{2+} alcohols via CO_2 hydrogenation by serving as the hydrogen source [31]. Despite the great progress and valuable insights from the above investigations, the details of the role of water in heterogeneous catalytic hydrogenation processes remain elusive.

For conjugated $C=O$ hydrogenation, the replacement of organic solvent with water has been proven available to improve both the activity and selectivity of Au and Pt catalysts [32,33]. Trace amounts of water have also been shown to enhance the activity on Pt-based catalysts [34]. The orientable chemisorption of the hydrophilic $C=O$ moiety in dipolar water solvent leads to satisfactory selectivity to unsaturated alcohol, according to the kinetic characterizations and adsorption spectra data [35–37]. Furthermore, isotopic-exchange studies have clarified the evolution of catalytically active sites in the pathway of direct hydrogenation by the dissociated H_2 [38,39]. The essential effect of water merits further investigation for selective hydrogenation on heterogeneous catalysts.

In this work, we employ carbon nanotube (CNT)-supported bimetallic PtFe nanoparticles (NPs) to efficiently achieve the chemoselective hydrogenation of cinnamaldehyde (CALD) to cinnamyl alcohol (CALA) with water as the only solvent. We illustrate the role of water as both a hydrogen carrier and a polar solvent by isotopic labeling experiments and theoretical calculations. The coexistence of two reaction pathways for water-mediated hydrogen exchange and dissociative hydrogenation with H_2 is also confirmed.

2. Experimental

2.1. Materials

Pt(acac)₂ (97.0%), Fe(acac)₃ (97.0%), benzyl alcohol (99.0%), cinnamaldehyde (CALD, 99.0%), phenylpropyl aldehyde (HCALD, 95.0%), cinnamyl alcohol (CALA, 98.0%), 3-phenylpropanol (HCALA, 99.0%), isopropanol (99.9%), n-heptane (98.0%), ethyl acetate (99.8%), cyclohexane (99.5%), and n-hexane (97.0%) were obtained from Sigma-Aldrich (Shanghai, China). HNO_3 (69%) and H_2SO_4 (98%) were provided by Aladdin Reagent Corp. (Shanghai, China). The deuterated solvent D_2O (deuteration degree > 99.8%) was provided by J&K Scientific (Shanghai, China). CO (99.99%), H_2 (99.999%), and Ar (99.999%) were supplied by Nanjing Special Gas Factory (Nanjing, China). Multiwalled carbon nanotubes (purity 97.1%, SBET 241 m^2/g , bulk density 0.05 g/cm^3) were purchased from CNano Technology (Zhenjiang, China).

2.2. Catalyst preparation

CNTs were chosen as the support due to their anchoring effect; the CNT surface with abundant oxygen-containing groups can stabilize the metallic sites via strong interactions. Supported Pt-based nanoparticle (NP) catalysts were prepared according to a modified procedure using benzyl alcohol and carbon monoxide as the co-reductant. The method affords a moderate size distribution of bimetallic NPs that have clean surfaces and do not contain residual organic ligands [40]. Consequently, the effects of the ligand can be ruled out, and the intrinsic activity of the Pt-based catalysts in water is truly reflected in the selective hydrogenation reaction.

2.2.1. Pretreatment of CNT support

The pristine CNTs were pretreated with concentrated HNO_3 at 120 °C for 4 h to remove impurities and to introduce surface

oxygen-containing groups to enhance the metal dispersion. The treated CNTs were washed with deionized water several times and dried in a 100 °C oven overnight. The CNT supports were kept dry before use.

2.2.2. Preparation of supported Pt-based catalysts

In a typical synthesis of the supported Pt catalyst, Pt(acac)₂ (100 mg, 0.25 mmol), 40 mL of benzyl alcohol and 800 mg of dry support were mixed together at room temperature and then stirred for 10 min. The resulting homogeneous yellow suspension was transferred to a glass pressure vessel. The sealed vessel was charged with 1 bar of CO gas and then heated for 3 h with vigorous stirring in an oil bath that had been preheated to 180 °C. After the vessel was cooled to room temperature, the catalyst was collected by centrifugation and washed several times with ethanol. For supported PtFe catalysts, the same preparation procedure was used and certain amounts of Pt(acac)₂ and Fe(acac)₃ were employed as metal precursors to obtain the desired Pt/Fe mole ratio. The Pt loadings were fixed at approximately 6.2 wt% for all Pt-based catalysts and confirmed by ICP-OES measurements. The identified real Pt/Fe ratios were 3.3, 8.5, and 58.7 for the Pt₃Fe/CNT, Pt₉Fe/CNT, and Pt₆₀Fe/CNT catalyst, respectively.

2.2.3. Acid washing of the Pt₃Fe/CNT catalyst

The reference catalyst was prepared via acid washing. The acid-washed sample without surface Fe species (Pt₃Fe/CNT- H_2SO_4) was obtained as follows: Pt₃Fe/CNT (100 mg) was soaked in 20 mL of H_2SO_4 (0.5 M) for 30 min, and the slurry was filtered and repeatedly washed with deionized water. Based on ICP-OES analysis, approximately 10% of the Fe has been removed, and the estimated Pt/Fe ratio of the Pt₃Fe/CNT- H_2SO_4 sample was 3.7.

2.3. Characterizations

The metal loadings for all catalysts were quantified using inductively coupled plasma optical emission spectrometry (ICP-OES, Avio 200, Perkin Elmer) by measuring the metal concentrations in solutions of the complexes dissolved in 40% hydrofluoric acid. X-ray diffraction (XRD) patterns were recorded on a Bruker AXS D8 Focus diffractometer using Ni-filtered $CuK\alpha$ radiation ($\lambda = 0.154$ nm) at 40 kV and 40 mA. Diffraction data were collected between 10° and 70° with a resolution of 0.02° (2 θ). Transmission electron microscopy (TEM) images were obtained on a JEOL JEM 3010 instrument operated at 300 kV. Scanning transmission electron microscopy (STEM) and elemental line scanning were carried out on an FEI Tecnai G² F20 S-TWIN system operated at 200 kV. X-ray photoelectron spectroscopy (XPS) measurements were acquired using a VG Scientific ESCALAB Mark II spectrometer equipped with two ultra-high-vacuum (UHV) chambers. All binding energies were referenced to the C1s peak at 284.6 eV.

2.4. Catalytic tests

Selective hydrogenations of CALD were carried out in a stainless steel reactor with a Teflon liner (Parr 4950, controller 4843). A 10-mg portion of catalyst, a certain amount of CALD (200, 400, or 1000 μL), and 10 mL of the solvent were added into the reactor. The molar ratio of CALD to total Pt atoms in the catalysts was approximately 500, 1000, or 2500, based on the CALD sampling amount. The residual air inside the reactor was expelled by pressurizing and releasing hydrogen several times. The reaction was performed at 60 °C under 20 bar of hydrogen. The stirring speed was set at 700 rpm for all the experiments in this study to eliminate the external mass transfer limitation. The equivalents of CALD, hydrogen pressure, and reaction temperature, as well as reaction time, were controlled in the tests of catalytic performance.

After the reactions were carried out in organic solvents, the catalyst powder was removed by centrifugation. For the reactions in water, in consideration of insoluble substances in water phase, ethyl acetate was added into the liner to thoroughly extract organic products and the solid catalyst was removed by centrifugation. All the products in the solution were analyzed using a gas chromatograph (GC, Agilent, 6890N) equipped with a CP-WAX 52 CB column (30 m × 0.25 mm × 0.25 μm) and a flame ionization detector (FID). Tetradecane was added as an internal standard. The byproducts were identified by gas chromatography–mass spectrometry (GCMS, Agilent, GC 6890N, MS 5973). The carbon balance was >98% in the hydrogenation reactions. We computed

$$\text{Conversion} = \{[N_{\text{in}}(\text{CALD}) - N_{\text{out}}(\text{CALD})]/N_{\text{in}}(\text{CALD})\} \times 100\%,$$

$$\text{Selectivity}(p-i) = N_{\text{out}}(p-i) / \sum_i N_{\text{out}}(p-i) \times 100\%,$$

$$\text{Carbon balance} = [N_{\text{out}}(\text{CALD}) + \sum_i N_{\text{out}}(p-i)] / N_{\text{in}}(\text{CALD}) \times 100\%,$$

$$\text{Specific reaction rate} = [V \times \rho \times \text{Conversion}/\text{MW}] / [\text{Time} \times N_{\text{total}}(\text{Pt})],$$

where $p-i$ represents hydrogenation products; $N(p-i)$ is the molar amount of the corresponding product i ; V , ρ , and MW are the sampling volume amount, density, and molecular weight for CALD, respectively; and $N_{\text{total}}(\text{Pt})$ is the molar number of total Pt atoms in employed catalyst.

The experimental CALD concentrations versus time are plotted according to a rate law that is first-order with respect to CALD, and the rate constant k is calculated from a regression fit of the experimental data:

$$\ln(C_t/C_0) = -k \times t,$$

where C_t represents the CALD concentration at reaction time t and C_0 is the initial CALD concentration.

Isotope studies were performed under similar reaction conditions except that deuterated solvent (D_2O) was used. For control experiments with/without the $\text{Pt}_3\text{Fe}/\text{CNT}$ catalyst, the substances for the standard hydrogenation reaction, including CALD and three kinds of main products (CALA, HCALD, and HCALA), were mixed with D_2O and stirred in a Parr reactor at 25 °C under 20 bar of N_2 for 24 h. The deuterated products were analyzed by GCMS and ^1H NMR (Bruker Advance 400 M).

2.5. Theoretical calculations

The structural model for the FePt surface in the present calculations was built based on previously reported characterization results for the Pt_3Fe NP catalysts [21]. Briefly, we used three-layered $\text{Pt}(111)$ surfaces to model the Pt substrate, and we

selected $\text{Fe}_6\text{O}_{18}\text{H}_{15}$ as a model for $\text{Fe}(\text{OH})_x$. Our calculations showed that $\text{Fe}_6\text{O}_{18}\text{H}_{15}$ can strongly anchor to the stepped surfaces of the $\text{Pt}(111)$ planes. First-principle calculations were carried out using the Vienna ab initio simulation package (VASP) based on the all-electron projected augmented wave (PAW) method [41,42]. The k -point sampling was generated following the Monkhorst–Pack procedure with a $2 \times 3 \times 1$ mesh. The Perdew–Wang 91 form of the generalized gradient approximation was used to calculate non-local gradient corrections to the correlation and exchange energies [43,44]. The GGA + U approximation with a U_{eff} of 3.0 eV for Fe atoms (antiferromagnetic) was used [44,45]. During structural optimization, the bottom layers of the slab were fixed at the bulk truncated position, while the top two layers and the adsorbates were fully relaxed. To prevent artificial interaction between the repeated slabs along the z -direction, a 15 Å vacuum was introduced with correction of the dipole moment. The reaction barriers were calculated using the climbing image nudged elastic band (CINEB) method [46,47]. The final transition state (TS) structures were refined using a quasi-Newton algorithm until the forces were less than 0.03 eV/Å.

3. Results and discussion

3.1. Catalyst structure

The XRD patterns (Fig. 1A) confirmed that the metallic NPs were well dispersed on the surfaces of CNT support. For all the catalysts, the (002) main diffraction at 25.8° suggested that the hexagonal graphite structure had been retained in the CNT support after the loading of the metals and pretreatment procedure of acid washing [48]. The diffraction peaks corresponding to the $\text{Pt}(111)$ and (200) planes at 39.6° and 46.1°, respectively, were observed for the Pt/CNT catalyst. For the bimetallic PtFe catalysts, these peaks gradually shifted to higher angles with increasing Fe loadings. Specifically, the peaks were located at 40.1° and 46.8° for the $\text{Pt}_3\text{Fe}/\text{CNT}$ catalyst. This indicated the formation of the PtFe alloy phase and was consistent with the unit cell shrinkage due to the smaller lattice parameter of Fe [49]. In addition, the alloy structure of the PtFe NPs in the $\text{Pt}_3\text{Fe}/\text{CNT}-\text{H}_2\text{SO}_4$ catalyst was maintained during acid washing with dilute H_2SO_4 .

The XPS studies confirmed that the Pt in the Pt-based catalysts was mainly reduced to metallic Pt^0 (Fig. 1B). The binding energies of 71.4 and 74.8 eV for the $\text{Pt}4f_{7/2}$ and $4f_{5/2}$ orbitals, respectively, were observed on the CNT-supported Pt and PtFe catalysts. Neither modifying Fe nor removing the oxygen-containing groups on the surfaces of the CNTs had a notable impact on the Pt binding energies. The signals from the $\text{Fe}2p_{3/2}$ orbitals were relatively weak; however, the coexistence of Fe^{2+} and Fe^{3+} species (55% vs. 45%) was observed for the $\text{Pt}_3\text{Fe}/\text{CNT}$ catalyst (Fig. 1C) [50].

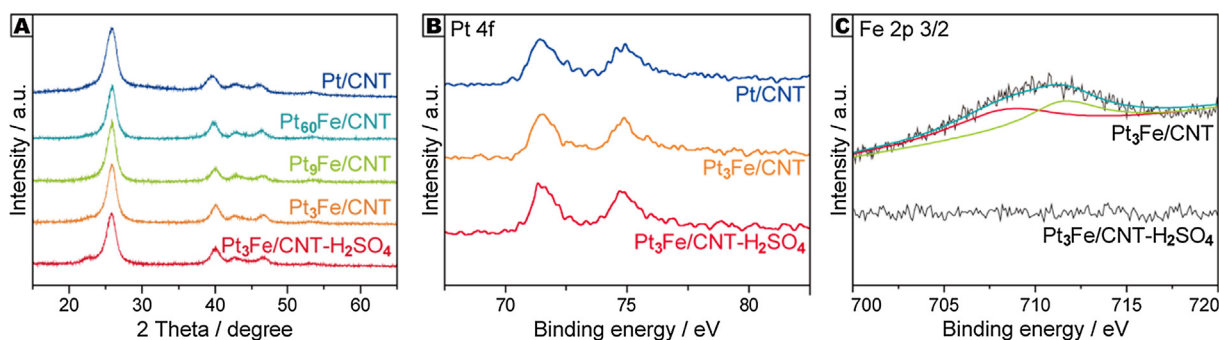


Fig. 1. (A) XRD patterns and (B, C) XPS spectra of Pt4f and Fe2p orbitals of various Pt and PtFe catalysts.

Furthermore, the disappearance of the Fe-related peaks in the XPS spectrum of the Pt₃Fe/CNT–H₂SO₄ catalyst confirmed the possibility of targeted removal of surface Fe species by acid washing pretreatment [51].

The TEM images of the Pt/CNT catalyst revealed that the CNT-supported monometallic Pt NPs are 2.7 ± 0.6 nm in particle size (Fig. 2A and B). With the modification of the second Fe metal, the sizes of PtFe NPs on CNT surfaces increased slightly in comparison with that of monometallic Pt NPs. As shown in Fig. 2C–H, the size distributions of PtFe NPs for Pt₆₀Fe, Pt₉Fe, and Pt₃Fe catalysts are 5.4 ± 1.3 , 5.4 ± 0.9 , and 6.7 ± 1.7 nm, respectively. STEM-EDX elemental line-scanning analysis was performed on various PtFe catalysts to further identify the formation of PtFe alloy structure. The compositional line profiles of Pt and Fe clearly cross individual

Pt₆₀Fe, Pt₉Fe, and Pt₃Fe particles, as illustrated in Fig. 2I–K. Accordingly, the ratio of the signal strength of Fe to Pt lines increased with the increasing Fe/Pt ratio from 1/60 to 1/3. The HRTEM images directly showed a lattice spacing of 0.23 nm, which corresponds to the (1 1 1) faces of Pt and PtFe alloys (Fig. 3A and B). Based on these characterization data, the CNT-supported PtFe NPs were composed of a PtFe alloy core and a shell comprising Fe oxide species.

3.2. Effects of the modification with Fe species

The selective hydrogenation of cinnamaldehyde (CALD) to cinnamyl alcohol (CALA) was performed on CNT-supported Pt and PtFe catalysts under relatively mild conditions (Fig. 4). The

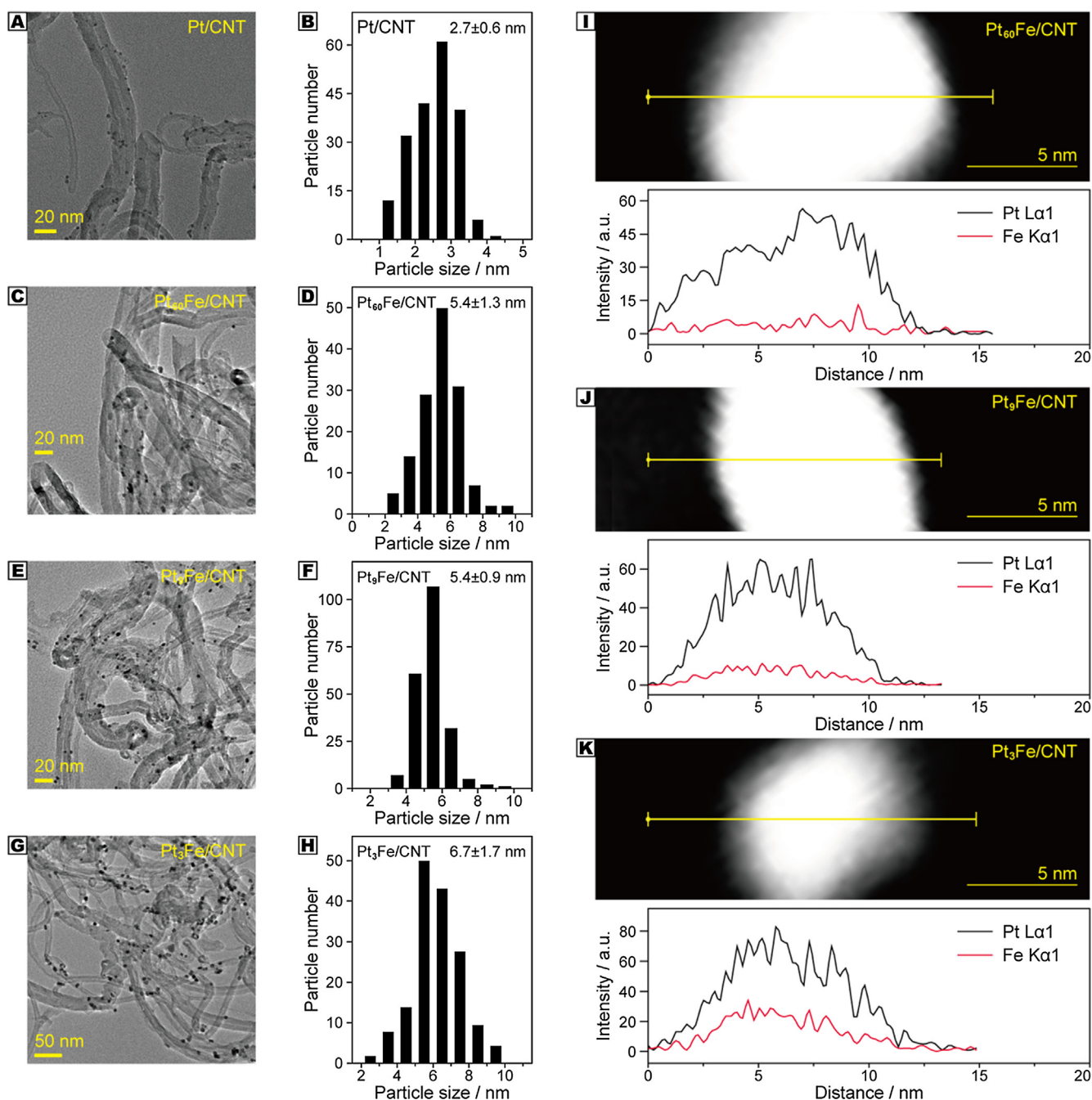


Fig. 2. TEM images and particle size distributions of CNT-supported Pt and PtFe catalysts (A–H); (I–K) STEM-EDX elemental line scanning profiles of PtFe NPs in PtFe/CNT catalysts.

catalytic performances in isopropanol, a common solvent for this reaction, are presented in Fig. 4A. To better judge the selectivity of the catalytic hydrogenation, a consistent level of CALD conversion (approximately 60%) over various catalysts was achieved by regulating the reaction times. The monometallic Pt/CNT showed an unsatisfactory CALA selectivity of 50.5%. The modification of Pt with Fe as a second metal dramatically enhanced the chemoselectivity for the C=O hydrogenation, and the addition of a sufficient amount of Fe was necessary for the enhancement. Specifically, the selectivity for CALA reached 95.5% at 60.9% conversion over the Pt₃Fe/CNT catalyst. The relationship between the specific reaction rate and the Pt/Fe ratio demonstrated that the alloyed PtFe could also boost the rate of the hydrogenation reaction as compared with the monometallic Pt/CNT catalyst. Furthermore, the variations in the performances with the Pt/Fe ratio indicated that the catalytic process was very sensitive to the structure of the PtFe NPs and the Pt–Fe interactions on the surface. On one hand, the electropositive Fe species could increase the electron density on the Pt to lower the probability of C=C activation and polarize the C=O

group for nucleophilic attack by the H species dissociated on the Pt site [52]. On the other hand, the oxidized Fe species may act as Lewis acidic sites and interact with the C=O group in CALD, promoting the selective conversion of CALD to CALA [34,53]. For instance, our previous work demonstrated that iron oxide nanosland-decorated Pt NPs displayed improved catalytic performances in the selective hydrogenation of CALD [54]. The specific Pt–FeO_x interfaces could also be generated by using atomic layer deposition, and the high selectivity for CALA was believed to be due to the precise blocking of low-coordinated Pt sites with Fe oxides [55].

It was reported that isopropanol could serve as a hydrogen donor in the transfer catalytic hydrogenation reactions [56,57]. A H₂-free blank hydrogenation reaction test in isopropanol was performed over a Pt₃Fe/CNT catalyst. CALD conversion less than 1% and CALA selectivity 48.9% were obtained under N₂. Such low selectivity suggested that the hydrogenation of CALD on Pt₃Fe/CNT catalyst may not follow the transfer hydrogenation pathway. The huge conversion gap also indicated that the direct

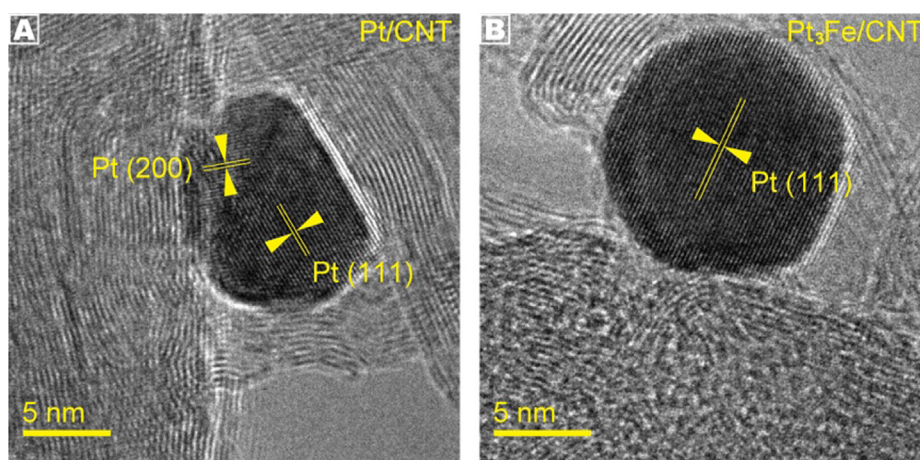


Fig. 3. HRTEM images of Pt/CNT and Pt₃Fe/CNT catalysts.

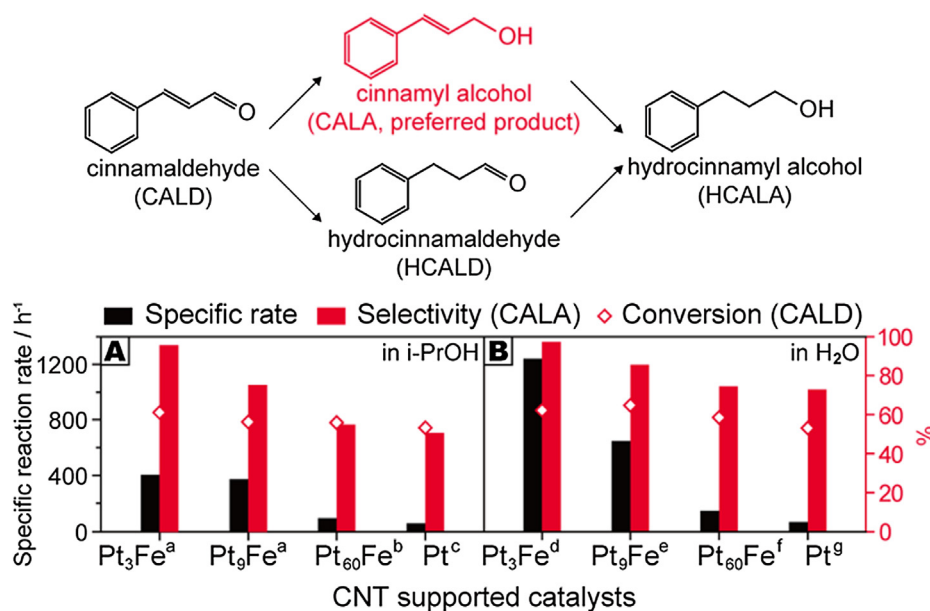


Fig. 4. Reaction network of CALD hydrogenation and the catalytic performances of the CNT-supported Pt-based catalysts in (A) isopropanol (i-PrOH) and (B) water. Reaction conditions: 10 mg of catalyst, 400 μ L of CALD, 10 mL of solvent, 20 bar of H₂, 60 $^{\circ}$ C, 700 rpm, and reaction time (a) 1.5 h; (b) 6 h; (c) 10 h; (d) 0.5 h; (e) 1 h; (f) 4 h; and (g) 8 h. The CALD conversions remained approximately 60% for all hydrogenation reactions.

hydrogenation overwhelmingly dominates the reaction process and isopropanol plays a solo role of solvent rather than hydrogen donor.

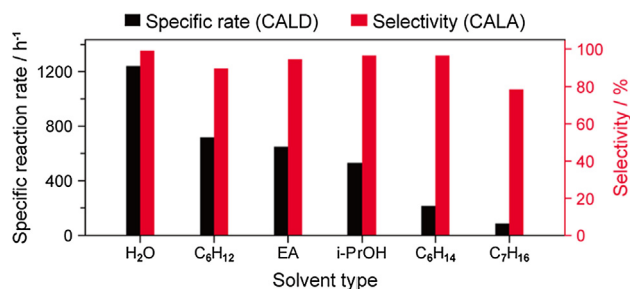


Fig. 5. The catalytic hydrogenation performance of Pt₃Fe/CNT catalysts in various solvents. The calculated specific reaction rate of CALD is based on the total molar amount of Pt atoms in Pt₃Fe/CNT catalyst. Reaction conditions: 10 mg of catalyst, 10 mL of solvent, 400 μ L of CALD, 20 bar of H₂, 60 $^{\circ}$ C, and 0.5 h. C₆H₁₂, EA, C₆H₁₄, and C₇H₁₆ represent cyclohexane, ethyl acetate, n-hexane, and n-heptane, respectively.

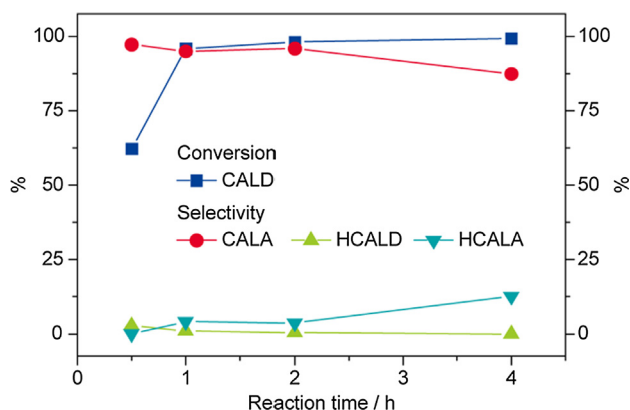


Fig. 6. The catalytic performance (CALD conversion and product selectivity) of Pt₃Fe/CNT as a function of reaction time. Reaction conditions: 10 mg of catalyst, 10 mL of H₂O, 400 μ L of CALD, 20 bar of H₂ and 60 $^{\circ}$ C.

3.3. Activity in water

The optimized Pt₃Fe/CNT catalyst was employed to explore the catalytic performance in CALD hydrogenation with pure water as the solvent. The activities and selectivities of Pt₃Fe/CNT catalyst in water and other types of organic solvents were first compared. Those solvents (e.g., cyclohexane and ethyl acetate) are frequently used in hydrogenation reactions of α,β -unsaturated aldehydes and ketones (Table S1 in the Supporting Information). As shown in Fig. 5, satisfactory CALD conversion and CALA selectivity were achieved in water as the solvent. It should be mentioned that the reaction rate of hydrogenation of the α,β -unsaturated aldehydes is not correlated with the hydrogen solubility, because the CALD conversion in isopropanol was less than half of that in water even though the solubility of H₂ in isopropanol is four times higher than that in water [58]. With the aid of water, the CALA selectivity of the Pt₃Fe/CNT catalyst further increased to 97.2%, while the conversion reached 62.1% in 0.5 h (Fig. 6). Such high selectivity (95.9%) was still observed at nearly complete conversion (98.1% in 1 h). The decline in the CALA selectivity in favor of the formation of the fully hydrogenated hydrocinnamyl alcohol (HCALA) suggested that the sequential hydrogenation of the C=O and C=C bonds occurred on the Pt₃Fe/CNT catalyst in water.

The facilitation effect of water was also observed in the hydrogenation reactions over Pt, Pt₉Fe, and Pt₆₀Fe catalysts (Fig. 4B). For instance, the CALA selectivity in water increased to 72.8% while the selectivity in isopropanol was 50.5% at the same level of conversion for the monometallic Pt/CNT catalyst. Slightly increased selectivity of CALA was also obtained in water on Pt₉Fe/CNT and Pt₆₀Fe/CNT catalysts, compared with that in isopropanol. In general, the polar water can substantially promote the adsorption and activation of hydrophilic C=O groups over C=C groups, thus producing CALA with a similar polarity [59]. However, we expect that this may not be the only role of water in this reaction process.

3.4. Water-involved hydrogen exchange

To further study the effects of water, pure deuterium oxide (D₂O) was used instead of H₂O to determine its effect on the

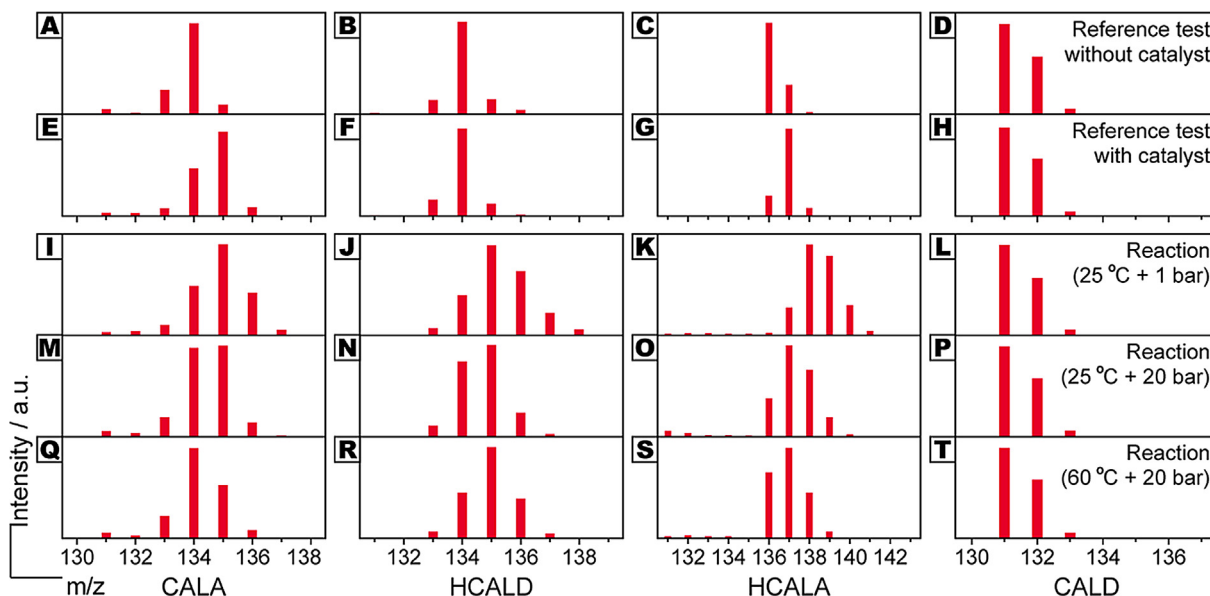


Fig. 7. The mass spectra of CALD and hydrogenation products in D₂O-labeling reactions with/without Pt₃Fe/CNT catalyst at different temperatures and H₂ pressures. (A–D) reference test without catalyst, (E–H) reference test with catalyst, (I–L) Pt₃Fe/CNT catalyzed reaction at 25 $^{\circ}$ C and 1 bar of H₂, (M–P) reaction at 25 $^{\circ}$ C and 20 bar of H₂, (Q–T) reaction at 60 $^{\circ}$ C and 20 bar of H₂.

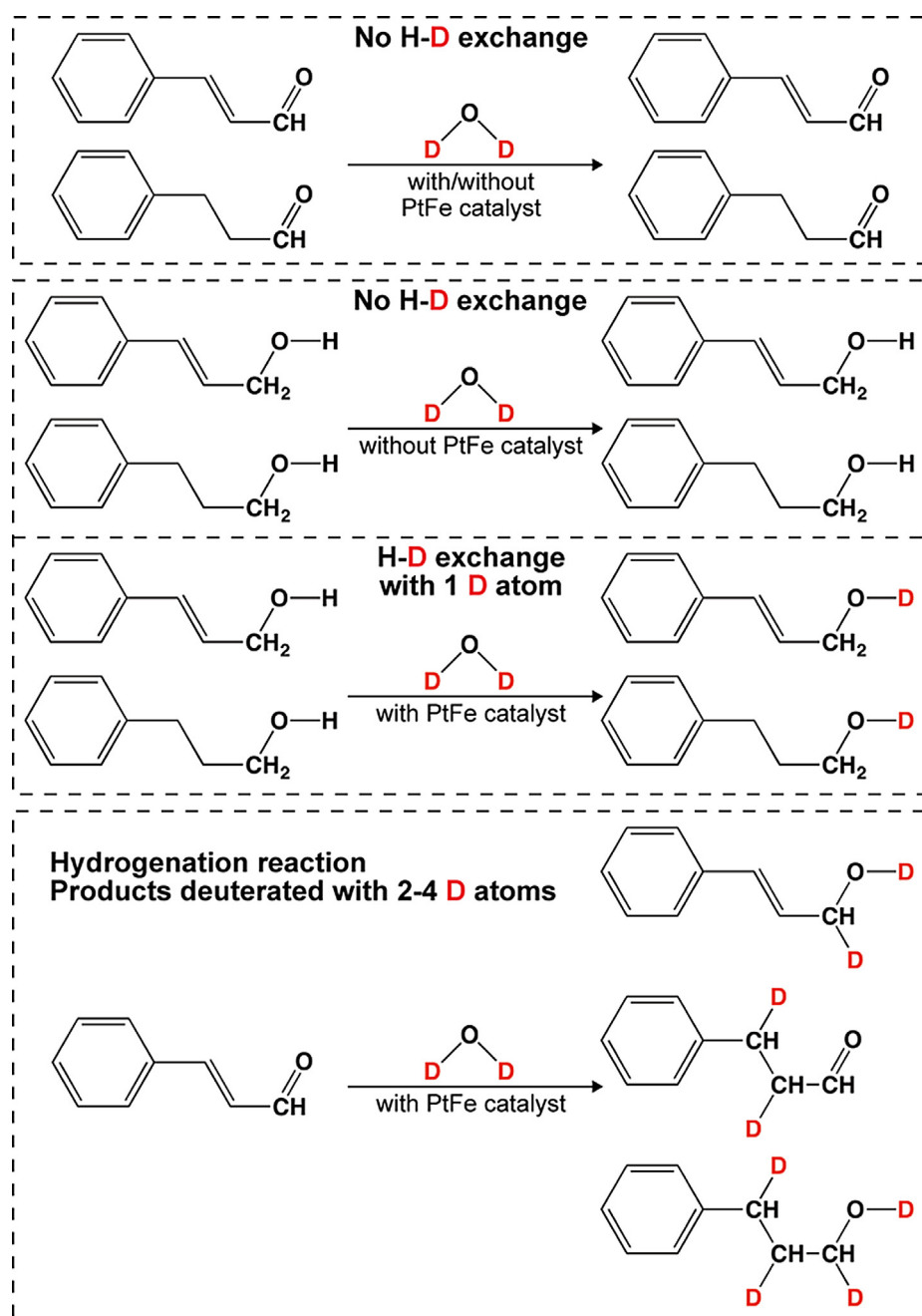
hydrogenation reaction catalyzed by Pt₃Fe/CNT. The exchange between D₂O and the related substances in the CALD hydrogenation reaction should be one of the first concerns. The reference test for the exchange process was carried out in the absence of the cat-

alyst and H₂. The H–D exchanges between the D atom in D₂O and the H atom in CALD and three kinds of main hydrogenation products (CALA, HCALD, and HCALA) were not favored without the catalyst, because only the regular molecular ion peak was observed on

Table 1
The performance of Pt₃Fe/CNT in H₂O/D₂O in the reaction of CALD hydrogenation.^a

Catalyst	Solvent	Temp. (°C)	P(H ₂) (bar)	CALD (μL)	Time (h)	Conv. (%)	Selec. CALA (%)	Selec. HCALD (%)	Selec. HCALA (%)
Pt ₃ Fe/CNT	H ₂ O	60	20	400	0.5	62.1	97.2	2.7	0.1
	D ₂ O				1	63.7	94.2	3.6	2.2
	D ₂ O	25	1	200	1	63.8	95.2	2.6	2.2
	D ₂ O				24	68.3	64.7	15.7	19.6

^a 10 mg catalyst, 10 mL solvent.



Scheme 1. The diagram of product distributions in the reference tests of substance–D₂O exchange with/without Pt₃Fe/CNT catalyst and the catalytic hydrogenation reaction in D₂O.

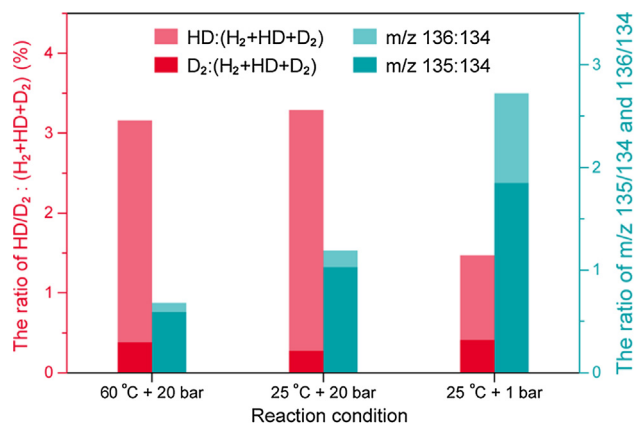


Fig. 8. Yields of gaseous D₂ and HD in H₂-D₂O exchange reaction and deuteriation degree of CALA in hydrogenation reaction catalyzed by Pt₃Fe/CNT.

GCMS spectra for the individual substances (Fig. 7A–D). The H₂-free exchange test was also performed in the presence of the Pt₃-Fe/CNT catalyst. No deuterated CALD and HCALD were detected by GCMS spectra, indicating that the alkenyl group and the aldehyde groups could not interact with molecular D₂O on the surface of the PtFe catalyst (Fig. 7F and H). The peak of *m/z* 135 for CALA and the peak of *m/z* 137 for HCALA were observed on GCMS spectra, which suggested that the H atom in the hydroxyl group preferred to exchange with the D atom in D₂O with the action of the PtFe catalyst (Fig. 7E and G). However, it should be noted that although the H–D exchange process was nearly completed, only one D atom was deuterated into the hydroxyl groups for all CALA and HCALA molecules. This suggested that α -C–H could not be exchanged with D₂O under the reaction condition.

The Pt₃Fe/CNT catalyzed hydrogenation reaction of CALD in D₂O was then performed and the details of the isotope studies are provided in Table 1. Analysis of the GCMS spectra revealed that the

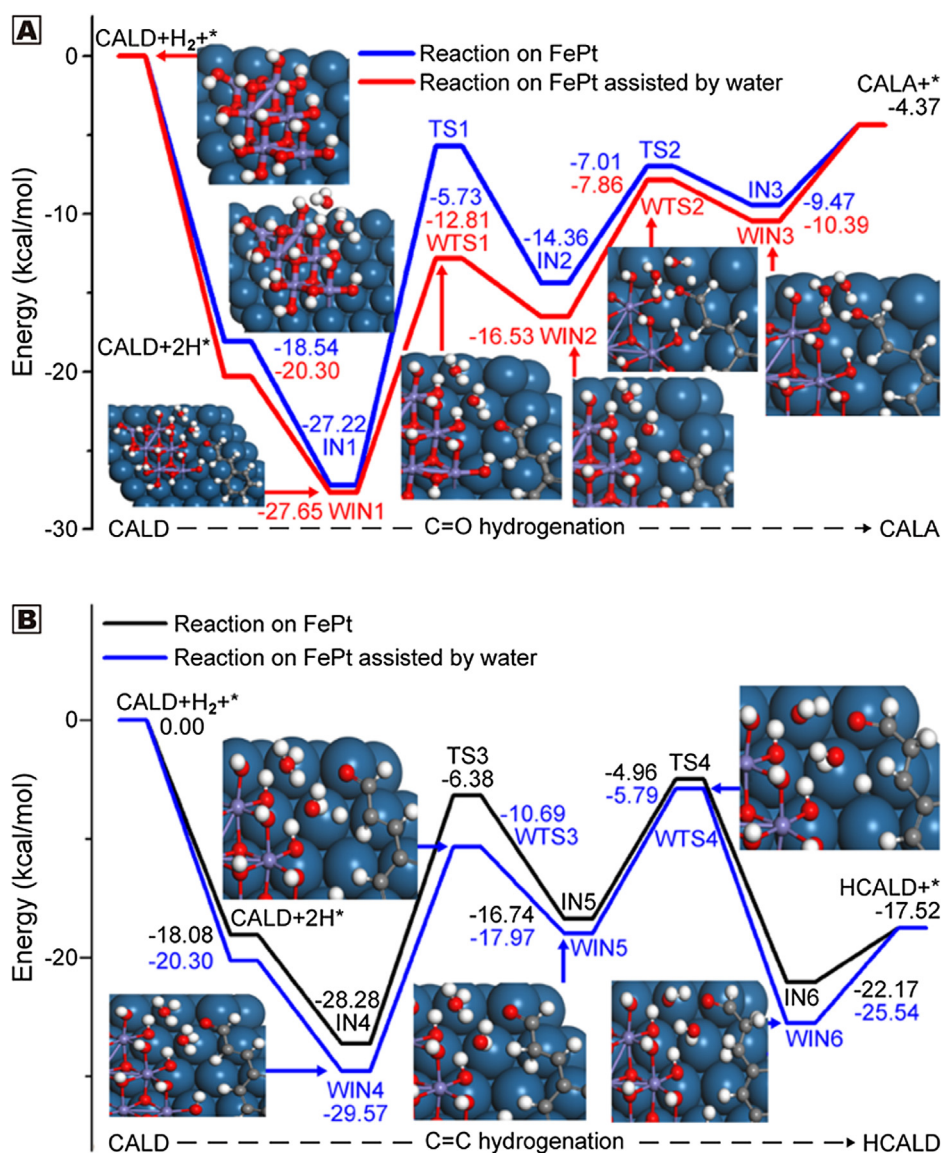
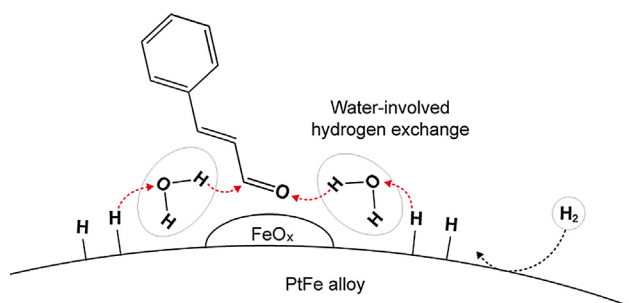


Fig. 9. The energetic profiles for the production of (A) CALA and (B) HCALD in the selective hydrogenation of CALD over the PtFe catalyst model with/without the assistance of water.

hydrogenation products were deuterated during the catalytic reaction (Fig. 7I–T). For the reaction at 25 °C and 1 bar of H₂, the molecular ion peaks at *m/z* 136 and 135 have clearly emerged in the GCMS spectrum of the CALA product, as shown in Fig. 7I, which suggested that both ends of the C=O bond in CALD were deuterated during the hydrogenation reaction. This result confirmed that it was a D₂O-involved reaction process rather than a simple H–D exchange process. Such a D₂O-involved process also occurred in the C=C hydrogenation reaction, which was supported by the fact that the peaks at *m/z* 138 and 137 and the coexisting peaks at *m/z* 140, 139, and 138 were observed on the GCMS spectra of HCALD and HCALA products, respectively (Fig. 7J and K). This result is summarized in Scheme 1, which strongly proves that D₂O was involved as a hydrogen exchange bridge in the selective hydrogenation of C=O and C=C bonds in CALD [60].

In consideration that the deuteration of products using HD or D₂ generated in situ from H₂–D₂O exchange on Pt catalyst may be one of the possible reaction pathways [61], the H₂–D₂O exchange reactions in the absence of CALD were also performed over Pt₃Fe/CNT catalyst. The yields of gaseous HD and D₂ produced from the H₂–D₂O exchange reaction and the deuteration degrees (the relative abundances for *m/z* 136, 135, and 134) of the CALA product in the D₂O-involved hydrogenation reaction could be compared under the same reaction conditions (e.g., temperatures, H₂ pressures, samplings, and times), as shown in Fig. 8. For H₂–D₂O exchange, similarly low yields of D₂ (approximately 0.3%) were observed under different reaction conditions, and the yield of HD at 25 °C and 1 bar of H₂ was much lower than that at 60 or 25 °C and 20 bar of H₂. This suggested that the reaction rate of exchange between H₂ and D₂O was mainly improved by the higher H₂ pressure in this temperature range. For the D₂O-involved hydrogenation reaction under a H₂ pressure of 20 bar, the ratio of the relative abundances of the peaks at *m/z* 135 and 136 to that at *m/z* 134 at 25 °C was obviously higher than that at 60 °C for CALA product (Fig. 7M and 7Q). When the reaction temperature was 25 °C, the peak at *m/z* 135 became dominant and the degree of deuteration was significantly increased under ambient H₂ pressure, in marked contrast to that under 20 bar (Fig. 7I and M). This suggested that much more D₂O actively and rapidly participated in the hydrogenation reaction at lower H₂ pressure and lower temperature. The reaction rate of H₂–D₂O exchange and the deuteration degree of CALA product in the hydrogenation reaction revealed the opposite trend with varied H₂ pressures and temperatures. In addition, the lower yield of HD and D₂ could not guarantee adequate supplies of D atoms to achieve such a higher deuteration degree of hydrogenation products. Therefore, as illustrated in Scheme 1, the D₂O-involved hydrogenation was neither a simple exchange process between D₂O and substances nor a tandem reaction process consisting of H₂–D₂O exchange reaction and deuteration reaction by HD or D₂ generated in situ.



Scheme 2. The schematic diagram of the reaction pathway of water-involved hydrogen exchange in the Pt₃Fe/CNT-catalyzed CALD hydrogenation.

The core role of water was examined by density functional theory (DFT) calculations for CALD hydrogenation over the PtFe surface model (details in Figs. S1–S3). As shown in Fig. 9, the assistance of water significantly decreases the energy barrier of the overall reaction, especially the energy barrier of the rate-determining step, for both the CALA and HCALD formation processes. However, even in the presence of water, noticeably lower activation energy barriers favored C=O hydrogenation over C=C hydrogenation on the PtFe surface (14.84 vs. 18.88 kcal/mol). This highlights the excellent synergetic effect between the water and the bimetallic PtFe NP catalysts in enhancing both the conversion of CALD and the selectivity for C=O hydrogenation. In contrast to the water-free formation of CALA, the water-mediated pathway had a much lower energy barrier (14.84 vs. 21.49 kcal/mol for WIN1-WTS1-WIN2 and IN1-TS1-IN2, respectively, in Fig. 9A). After

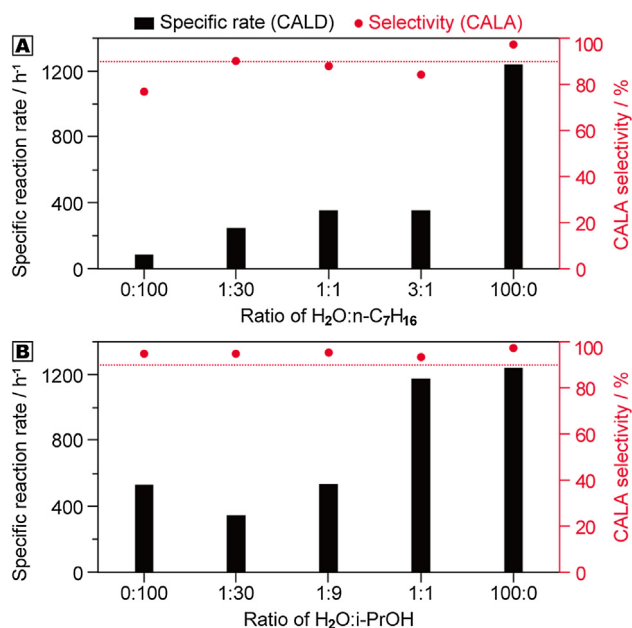


Fig. 10. The catalytic performance of the Pt₃Fe/CNT catalyst in mixtures of (A) n-heptane–water and (B) isopropanol–water. Reaction conditions: 10 mg of catalyst, 400 μ L of CALD, 60 °C, 20 bar H₂, 10 mL solvent, 0.5 h.

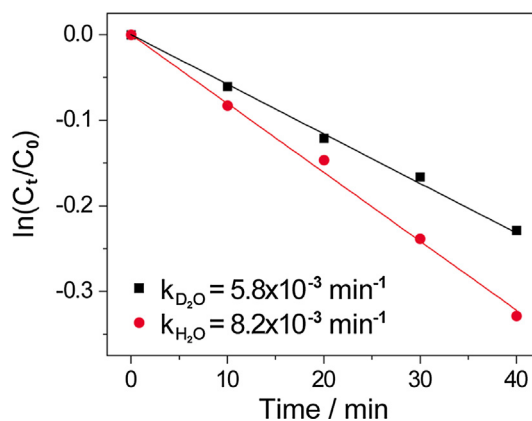


Fig. 11. The reaction rate constants (*k*) of Pt₃Fe/CNT-catalyzed CALD hydrogenation in H₂O and D₂O. C₀ represents the initial molar concentration of CALD while C_t represents the molar concentration of CALD varied with reaction time. The reaction conditions: 10 mg of catalyst, 1.0 mL of CALD, 10 mL solvent, 20 bar H₂, 60 °C. For all reaction tests, the conversion and the CALA selectivity stayed at <25% and >92%, respectively.

the co-adsorption of CALD and dissociated H atoms on the surface of the catalyst, the water initially attached to the Pt–H surface and the O atom of the CALD species via two hydrogen bonds, acting as a hydrogen bridge. The water-assisted hydrogen exchange process was then achieved. Complete abstraction of the H atom from the Pt surface generated a bond with the O atom in H₂O, while the O–H bond on the other side of the H₂O broke and the H atom transferred into the hydrogenation product, producing H-exchanged H₂O and CALA, as shown in Scheme 2.

Water-involved hydrogen exchange is apparently affected by the hydrogen bonding interactions between the H₂O, CALD, and Pt sites. To elucidate their mechanism of influence, we created two mixed solvent systems, H₂O–n-heptane and H₂O–isopropanol, with different combinations of hydrogen bonds. Fig. 10A shows that the conversion rate of CALD increased proportionally with the ratio of water to heptane over the Pt₃Fe/CNT catalyst. However,

the reaction rate initially decreased and then increased as the water/isopropanol ratio increased (Fig. 10B). This clearly indicated that the interactions between polar solvent molecules could competitively interrupt the hydrogen bonding interactions in the water-involved hydrogen exchange and thus influence the CALD conversion.

For Pt₃Fe/CNT-catalyzed CALD hydrogenation, the reaction rate constants (*k*) in H₂O and D₂O were analyzed in the initial reaction stages. $\ln(C_t/C_0)$ was plotted as a first-order function of reaction time with respect to CALD, as shown in Fig. 11. k_{H_2O} and k_{D_2O} are $8.2 \times 10^{-3} \text{ min}^{-1}$ and $5.8 \times 10^{-3} \text{ min}^{-1}$, respectively, and the ratio of k_{H_2O} to k_{D_2O} is only 1.4. This result suggested that the kinetic isotope effect existed in the catalytic hydrogenation reaction with the involvement of D₂O; however, the cleavage of O–H bonds in H₂O and subsequent hydrogen exchange were not the rate-determining steps. This accords with the result from DFT calculations that the H₂O-bridged hydrogen-exchange process easily occurs with a relatively low energy barrier.

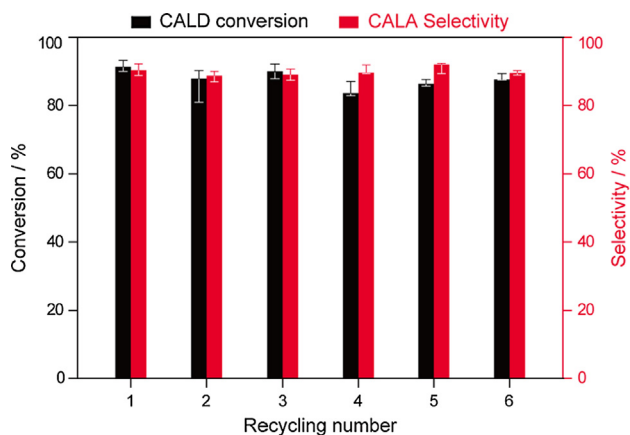


Fig. 12. Recycling stability of the Pt₃Fe/CNT catalyst in the selective hydrogenation of CALD in water as the solvent. Reaction conditions: 10 mg catalyst, 10 mL H₂O, 200 μ L CALD, 20 bar H₂, 60 °C, 1 h.

3.5. Reusability of Pt₃Fe/CNT in water

The presence of stable Fe³⁺ and Fe²⁺ species on the surface of the Pt₃Fe NPs was of great importance for both the catalytic activity and the hydrogenation selectivity. When oxidized Fe species were eliminated from the surfaces of the NPs by acid washing with dilute H₂SO₄, the CALD conversion after the same reaction time fell to half of its initial value (Fig. S4). At a similar level of CALD conversion, the selectivity for CALA had decreased slightly with the Pt₃Fe/CNT–H₂SO₄ catalyst, unlike that with the fresh Pt₃Fe/CNT catalyst. However, the Pt₃Fe/CNT–H₂SO₄ catalyst still showed a higher CALA selectivity and a conversion twice as high as what was achieved with the monometallic Pt/CNT catalyst, and this may have been due to the stability of the PtFe alloy in the bulk NPs [53,62].

The stability and reusability tests for the Pt₃Fe/CNT catalyst in water were performed repeatedly, and the results are shown in Fig. 12. After each reaction run, the catalyst was separated from

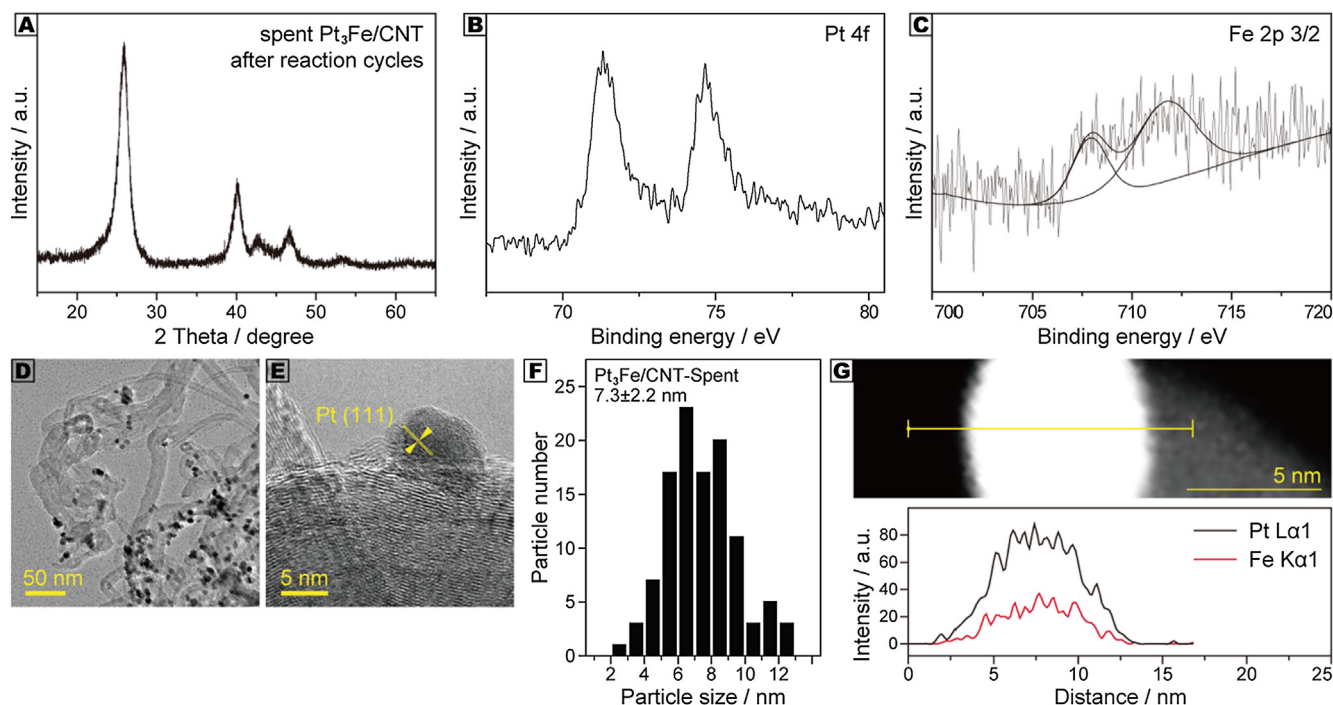


Fig. 13. (A) XRD pattern, (B, C) XPS Pt4f and Fe2p spectra, (D, E) TEM and HRTEM images, (F) particle size distribution, and (G) STEM-EDX elemental line-scanning profiles of the spent Pt₃Fe/CNT catalyst after six-cycle hydrogenation reaction.

the mixture, washed with ethanol several times, and then dried overnight. There was a slight fluctuation in both the CALD conversion and the CALA selectivity in the recycling runs. A CALD conversion of 87.5% and a CALA selectivity of 90.3% were maintained even after six runs, indicating good recyclability of the Pt₃Fe/CNT catalyst for the selective hydrogenation of CALD in water.

The structure of the recycled Pt₃Fe/CNT catalyst was examined by a series of characterization techniques, and no marked variations were observed. In addition, no leaching of Fe into the reaction solution was detected. Both the alloy structure and the moderate crystal size of the PtFe NPs were maintained, which was reflected in the XRD pattern of the spent catalyst (Fig. 13A). The XPS spectra suggested that Pt was kept in the metallic Pt⁰ state, as shown in Fig. 13B. Surface Fe species were still present as both Fe²⁺ and Fe³⁺; however, the Fe³⁺/Fe²⁺ ratio increased during the hydrogenation reaction (31% Fe²⁺ and 69% Fe³⁺, Fig. 13C). The transformation of Fe²⁺ to Fe³⁺ suggested that the electron-donating process occurred on the Fe²⁺ sites in the hydrogenation reaction. The TEM and HRTEM images revealed that the Pt₃Fe NPs on the CNT surface slightly grew to 7.3 ± 2.2 nm from 6.7 ± 1.7 nm after six reaction runs (Fig. 13D–F). The STEM-EDX elemental line-scanning profiles (Fig. 13G) confirmed that the core structure of Pt₃Fe alloy NPs was well preserved.

To further study whether water-involved hydrogen exchange occurs steadily in the hydrogenation of CALD, alternating reactions were run in H₂O and D₂O. The reactions were performed at 25 °C and 1 bar of H₂, and the products were analyzed by GC–MS. As illustrated in Fig. 14, when D₂O was used instead of H₂O as the sol-

vent, the main molecular ion peak in MS spectra from the CALA product was *m/z* 135 rather than *m/z* 134, which strongly confirmed the participation of D₂O in the reaction system. In the fourth run, the intensity of the peak at *m/z* 135 did not change, suggesting that the water-involved hydrogen exchange was a stable reaction pathway in the hydrogenation of CALD.

4. Conclusions

In summary, we demonstrated that supported PtFe NPs can efficiently catalyze the hydrogenation of cinnamaldehyde to cinnamyl alcohol with high selectivity (>97%) under relatively mild reaction conditions with pure water as the solvent. By conducting a combination of experimental and theoretical studies, we confirmed that the pathway of water-involved hydrogen exchange was active during the catalytic reaction, and this pathway coexisted with direct hydrogenation with dissociated H₂. The water molecule acts as a bridge to facilitate hydrogen exchange between the CALD species and the Pt sites with lower thermodynamic energy barriers. We expect that the strategy of exploiting the synergistic effects of water and metallic catalysts could be adopted to explore novel catalytic systems for the development of selective hydrogenation processes.

See Figs. S1–S4 and Table S1 for DFT calculation details and comparison of catalytic performances.

Acknowledgments

We are grateful for financial support from the Jiangsu Provincial Department of Education and Natural Science Foundation (17KJB150021 and BK20170986) and partial support from the National Natural Science Foundation of China (21503187). We also appreciate the support from Nanjing Tech University and a SICAM Fellowship from the Jiangsu National Synergetic Innovation Center for Advanced Materials. We thank Dr. Shihui Zou and Professor Jie Fan for assistance with the STEM-EDX analysis.

Appendix A. Supplementary material

Supplementary data associated with this article can be found, in the online version, at <https://doi.org/10.1016/j.jcat.2018.05.008>.

References

- [1] P. Gallezot, D. Richard, Selective hydrogenation of α , β -unsaturated aldehydes, *Catal. Rev.* 40 (1998) 81–126.
- [2] C. Vriamont, T. Haynes, E. McCague-Murphy, F. Pennetreau, O. Riant, S. Hermans, Covalently and non-covalently immobilized clusters onto nanocarbons as catalysts precursors for cinnamaldehyde selective hydrogenation, *J. Catal.* 329 (2015) 389–400.
- [3] K.-H. Dostert, C.P. O'Brien, F. Ivars-Barceló, S. Schauerermann, H.-J. Freund, Spectators control selectivity in surface chemistry: acrolein partial hydrogenation over Pd, *J. Am. Chem. Soc.* 137 (2015) 13496–13502.
- [4] G. Kennedy, L.R. Baker, G.A. Somorjai, Selective amplification of CO bond hydrogenation on Pt/TiO₂: catalytic reaction and sum-frequency generation vibrational spectroscopy studies of crotonaldehyde hydrogenation, *Angew. Chem. Int. Ed.* 53 (2014) 3405–3408.
- [5] B. Wu, H. Huang, J. Yang, N. Zheng, G. Fu, Selective hydrogenation of α , β -unsaturated aldehydes catalyzed by amine-capped platinum-cobalt nanocrystals, *Angew. Chem. Int. Ed.* 51 (2012) 3440–3443.
- [6] Y. Zhu, H. Qian, B.A. Drake, R. Jin, Atomically Precise Au₂₅(SR)₁₈ nanoparticles as catalysts for the selective hydrogenation of α , β -unsaturated ketones and aldehydes, *Angew. Chem. Int. Ed.* 49 (2010) 1295–1298.
- [7] E. Castillejos, P.-J. Debouttière, L. Roiban, A. Solhy, V. Martinez, Y. Kihn, O. Ersen, K. Philippot, B. Chaudret, P. Serp, An efficient strategy to drive nanoparticles into carbon nanotubes and the remarkable effect of confinement on their catalytic performance, *Angew. Chem. Int. Ed.* 48 (2009) 2529–2533.
- [8] H. Lin, J. Zheng, X. Zheng, Z. Gu, Y. Yuan, Y. Yang, Improved chemoselective hydrogenation of crotonaldehyde over bimetallic AuAg/SBA-15 catalyst, *J. Catal.* 330 (2015) 135–144.

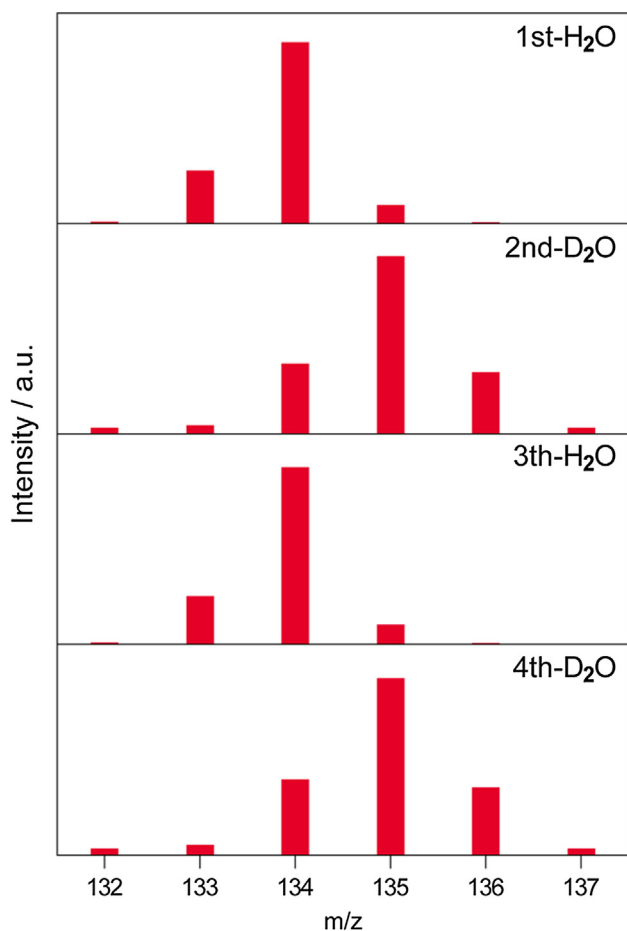


Fig. 14. Mass spectra of CALA product in Pt₃Fe/CNT-catalyzed hydrogenation reaction runs using H₂O and D₂O as solvent. Reaction conditions: 10 mg catalyst, 200 μ L CALD, 10 mL solvent, 1 bar H₂, 25 °C, and 1 h.

- [9] H. Yin, S. Zhao, K. Zhao, A. Muqsit, H. Tang, L. Chang, H. Zhao, Y. Gao, Z. Tang, Ultrathin platinum nanowires grown on single-layered nickel hydroxide with high hydrogen evolution activity, *Nat. Commun.* 6 (2015) 6430.
- [10] Y. Dai, Y. Wang, B. Liu, Y. Yang, Metallic nanocatalysis: an accelerating seamless integration with nanotechnology, *Small* 11 (2015) 268–289.
- [11] W.O. Oduro, N. Cailuo, K.M.K. Yu, H. Yang, S.C. Tsang, Geometric and electronic effects on hydrogenation of cinnamaldehyde over unsupported Pt-based nanocrystals, *Phys. Chem. Chem. Phys.* 13 (2011) 2590–2602.
- [12] S.C. Tsang, N. Cailuo, W. Oduro, A.T.S. Kong, L. Clifton, K.M.K. Yu, B. Thiebaut, J. Cookson, P. Bishop, Engineering preformed cobalt-doped platinum nanocatalysts for ultrasensitive hydrogenation, *ACS Nano* 2 (2008) 2547–2553.
- [13] Y. Zhu, F. Zaera, Selectivity in the catalytic hydrogenation of cinnamaldehyde promoted by Pt/SiO₂ as a function of metal nanoparticle size, *Catal. Sci. Technol.* 4 (2014) 955–962.
- [14] K.R. Kahsar, D.K. Schwartz, J.W. Medlin, Control of metal catalyst selectivity through specific noncovalent molecular interactions, *J. Am. Chem. Soc.* 136 (2014) 520–526.
- [15] Z. Guo, C. Xiao, R.V. Maligal-Ganesh, L. Zhou, T.W. Goh, X. Li, D. Tesfagaber, A. Thiel, W. Huang, Pt nanoclusters confined within metal-organic framework cavities for chemoselective cinnamaldehyde hydrogenation, *ACS Catal.* 4 (2014) 1340–1348.
- [16] M. Zhao, K. Yuan, Y. Wang, G. Li, J. Guo, L. Gu, W. Hu, H. Zhao, Z. Tang, Metal-organic frameworks as selectivity regulators for hydrogenation reactions, *Nature* 539 (2016) 76–80.
- [17] M. Zhao, K. Deng, L. He, Y. Liu, G. Li, H. Zhao, Z. Tang, Core-shell palladium nanoparticle@Metal-organic frameworks as multifunctional catalysts for cascade reactions, *J. Am. Chem. Soc.* 136 (2014) 1738–1741.
- [18] M.-O. Simon, C.-J. Li, Green chemistry oriented organic synthesis in water, *Chem. Soc. Rev.* 41 (2012) 1415–1427.
- [19] J. Fester, M. García-Melchor, A.S. Walton, M. Bajdich, Z. Li, L. Lammich, A. Vojvodic, J.V. Lauritsen, Edge reactivity and water-assisted dissociation on cobalt oxide nanoislands, *Nat. Commun.* 8 (2017) 14169.
- [20] A.M. Abdel-Mageed, S. Eckle, R.J. Behm, High selectivity of supported Ru catalysts in the selective CO methanation-water makes the difference, *J. Am. Chem. Soc.* 137 (2015) 8672–8675.
- [21] G. Chen, Y. Zhao, G. Fu, P.N. Duchesne, L. Gu, Y. Zheng, X. Weng, M. Chen, P. Zhang, C.-W. Pao, J.-F. Lee, N. Zheng, Interfacial effects in iron-nickel hydroxide-platinum nanoparticles enhance catalytic oxidation, *Science* 344 (2014) 495–499.
- [22] Y. Yang, C.A. Mims, D.H. Mei, C.H.F. Peden, C.T. Campbell, Mechanistic studies of methanol synthesis over Cu from CO/CO₂/H₂/H₂O mixtures: the source of C in methanol and the role of water, *J. Catal.* 298 (2013) 10–17.
- [23] B.N. Zope, D.D. Hibbitts, M. Neurock, R.J. Davis, Reactivity of the gold/water interface during selective oxidation catalysis, *Science* 330 (2010) 74–78.
- [24] C.-R. Chang, Z.-Q. Huang, J. Li, The promotional role of water in heterogeneous catalysis: Mechanism insights from computational modeling, *WIREs Comput. Mol. Sci.* 6 (2016) 679–693.
- [25] D.D. Hibbitts, B.T. Loveless, M. Neurock, E. Iglesia, Mechanistic role of water on the rate and selectivity of Fischer-Tropsch synthesis on ruthenium catalysts, *Angew. Chem. Int. Ed.* 52 (2013) 12273–12278.
- [26] L. Yang, Y. Choi, W. Qin, H. Chen, K. Blinn, M. Liu, P. Liu, J. Bai, T.A. Tyson, M. Liu, Promotion of water-mediated carbon removal by nanostructured barium oxide/nickel interfaces in solid oxide fuel cells, *Nat. Commun.* 2 (2011) 357.
- [27] S. Liu, R. Ohnishi, M. Ichikawa, Promotional role of water added to methane feed on catalytic performance in the methane dehydroaromatization reaction on Mo/HZSM-5 catalyst, *J. Catal.* 220 (2003) 57–65.
- [28] C. Wang, X.-K. Gu, H. Yan, Y. Lin, J. Li, D. Liu, W.-X. Li, J. Lu, Water-mediated Mars-Van Krevelen mechanism for CO oxidation on ceria-supported single-atom Pt₁ catalyst, *ACS Catal.* 7 (2017) 887–891.
- [29] M. Daté, M. Okumura, S. Tsubota, M. Haruta, Vital role of moisture in the catalytic activity of supported gold nanoparticles, *Angew. Chem. Int. Ed.* 43 (2004) 2129–2132.
- [30] L.R. Merte, G. Peng, R. Bechstein, F. Rieboldt, C.A. Farberow, L.C. Grabow, W. Kudernatsch, S. Wendt, E. Lægsgaard, M. Mavrikakis, F. Besenbacher, Water-mediated proton hopping on an iron oxide surface, *Science* 336 (2012) 889–893.
- [31] Z. He, Q. Qian, J. Ma, Q. Meng, H. Zhou, J. Song, Z. Liu, B. Han, Water-enhanced synthesis of higher alcohols from CO₂ hydrogenation over a Pt/Co₃O₄ catalyst under milder conditions, *Angew. Chem. Int. Ed.* 55 (2016) 737–741.
- [32] M.-M. Wang, L. He, Y.-M. Liu, Y. Cao, H.-Y. He, K.-N. Fan, Gold supported on mesostructured ceria as an efficient catalyst for the chemoselective hydrogenation of carbonyl compounds in neat water, *Green Chem.* 13 (2011) 602–607.
- [33] X. Xiang, W. He, L. Xie, F. Li, A mild solution chemistry method to synthesize hydroxalcite-supported platinum nanocrystals for selective hydrogenation of cinnamaldehyde in neat water, *Catal. Sci. Technol.* 3 (2013) 2819–2827.
- [34] Z. Guo, Y. Chen, L. Li, X. Wang, G.L. Haller, Y. Yang, Carbon nanotube-supported Pt-based bimetallic catalysts prepared by a microwave-assisted polyol reduction method and their catalytic applications in the selective hydrogenation, *J. Catal.* 276 (2010) 314–326.
- [35] J. Hidalgo-Carrillo, M.A. Aramendía, A. Marinas, J.M. Marinas, F.J. Urbano, Support and solvent effects on the liquid-phase chemoselective hydrogenation of crotonaldehyde over Pt catalysts, *Appl. Catal. A Gen.* 385 (2010) 190–200.
- [36] H.G. Manyar, D. Weber, H. Daly, J.M. Thompson, D.W. Rooney, L.F. Gladden, E. Hugh Stitt, J. Jose Delgado, S. Bernal, C. Hardacre, Deactivation and regeneration of ruthenium on silica in the liquid-phase hydrogenation of butan-2-one, *J. Catal.* 265 (2009) 80–88.
- [37] S.-I. Fujita, Y. Sano, B.M. Bhanage, M. Arai, Supported liquid-phase catalysts containing ruthenium complexes for selective hydrogenation of α , β -unsaturated aldehyde: Importance of interfaces between liquid film, solvent, and support for the control of product selectivity, *J. Catal.* 225 (2004) 95–104.
- [38] A. Chambers, S. David Jackson, D. Stirling, G. Webb, Selective Hydrogenation of cinnamaldehyde over supported copper catalysts, *J. Catal.* 168 (1997) 301–314.
- [39] H. Yoshitake, Y. Iwasawa, Cooperative behavior of two kinds of reaction sites and reaction mechanisms for deuteration of acrolein on SMSI-Pt/Nb₂O₅ catalyst, *J. Catal.* 125 (1990) 227–242.
- [40] G. Chen, Y. Tan, B. Wu, G. Fu, N. Zheng, Carbon monoxide-controlled synthesis of surface-clean Pt nanoclusters with high electrocatalytic activity, *Chem. Commun.* 48 (2012) 2758–2760.
- [41] G. Kresse, J. Furthmüller, Efficient iterative schemes for ab initio total-energy calculations using a plane-wave basis set, *Phys. Rev. B* 54 (1996) 11169–11186.
- [42] G. Kresse, J. Hafner, Ab initio, *Phys. Rev. B* 48 (1993) 13115–13118.
- [43] J.P. Perdew, J.A. Chevary, S.H. Vosko, K.A. Jackson, M.R. Pederson, D.J. Singh, C. Fiolhais, Atoms, molecules, solids, and surfaces: applications of the generalized gradient approximation for exchange and correlation, *Phys. Rev. B* 46 (1992) 6671–6687.
- [44] L. Giordano, G. Pacchioni, J. Goniakowski, N. Nilius, E.D.L. Rienks, H.-J. Freund, Interplay between structural, magnetic, and electronic properties in a FeO/Pt (111) ultrathin film, *Phys. Rev. B* 76 (2007) 075416.
- [45] W. Zhang, Z. Li, Y. Luo, J. Yang, First principles study on the geometric and electronic structures of the FeO/Pt(111) surface, *J. Phys. Chem. C* 113 (2009) 8302–8305.
- [46] G. Henkelman, B.P. Uberuaga, H. Jónsson, A climbing image nudged elastic band method for finding saddle points and minimum energy paths, *J. Chem. Phys.* 113 (2000) 9901–9904.
- [47] M. Ritter, W. Ranke, W. Weiss, Growth and structure of ultrathin FeO films on Pt(111) studied by STM and LEED, *Phys. Rev. B* 57 (1998) 7240–7251.
- [48] Z.-T. Liu, C.-X. Wang, Z.-W. Liu, J. Lu, Selective hydrogenation of cinnamaldehyde over Pt-supported multi-walled carbon nanotubes: Insights into the tube-size effects, *Appl. Catal. A Gen.* 344 (2008) 114–123.
- [49] Q. Fu, W.-X. Li, Y. Yao, H. Liu, H.-Y. Su, D. Ma, X.-K. Gu, L. Chen, Z. Wang, H. Zhang, B. Wang, X. Bao, Interface-confined ferrous centers for catalytic oxidation, *Science* 328 (2010) 1141–1144.
- [50] T.-C. Lin, G. Seshadri, J.A. Kelber, A consistent method for quantitative XPS peak analysis of thin oxide films on clean polycrystalline iron surfaces, *Appl. Surf. Sci.* 119 (1997) 83–92.
- [51] C. Zhou, Y. Chen, Z. Guo, X. Wang, Y. Yang, Promoted aerobic oxidation of benzyl alcohol on CNT supported platinum by iron oxide, *Chem. Commun.* 47 (2011) 7473–7475.
- [52] S. Galvagno, A. Donato, G. Neri, R. Pietropaolo, D. Pietropaolo, Hydrogenation of cinnamaldehyde over platinum catalysts: influence of addition of metal chlorides, *J. Mol. Catal.* 49 (1989) 223–232.
- [53] N. Mahata, F. Gonçalves, M.F.R. Pereira, J.L. Figueiredo, Selective hydrogenation of cinnamaldehyde to cinnamyl alcohol over mesoporous carbon supported Fe and Zn promoted Pt catalyst, *Appl. Catal. A Gen.* 339 (2008) 159–168.
- [54] Z. Guo, C. Zhou, D. Shi, Y. Wang, X. Jia, J. Chang, A. Borgna, C. Wang, Y. Yang, Toward the decoration of Pt nanoparticles supported on carbon nanotubes with Fe oxides and its effect on the catalytic reaction, *Appl. Catal. A Gen.* 435–436 (2012) 131–140.
- [55] Q. Hu, S. Wang, Z. Gao, Y. Li, Q. Zhang, Q. Xiang, Y. Qin, The precise decoration of Pt nanoparticles with Fe oxide by atomic layer deposition for the selective hydrogenation of cinnamaldehyde, *Appl. Catal. B Environ.* 218 (2017) 591–599.
- [56] D. Wang, D. Astruc, The Golden Age of Transfer Hydrogenation, *Chem. Rev.* 115 (2015) 6621–6686.
- [57] Q. Zhang, S.-S. Li, M.-M. Zhu, Y.-M. Liu, H.-Y. He, Y. Cao, Direct reductive amination of aldehydes with nitrorenes using bio-renewable formic acid as a hydrogen source, *Green Chem.* 18 (2016) 2507–2513.
- [58] J. Häjek, N. Kumar, P. Mäki-Arvela, T. Salmi, D.Y. Murzin, I. Paseka, T. Heikkilä, E. Laine, P. Laukkanen, J. Väyrynen, Ruthenium-modified MCM-41 mesoporous molecular sieve and Y zeolite catalysts for selective hydrogenation of cinnamaldehyde, *Appl. Catal. A Gen.* 251 (2003) 385–396.
- [59] P. Mäki-Arvela, L.-P. Tiainen, A.K. Neyestanani, R. Sjöholm, T.-K. Rantakylä, E. Laine, T. Salmi, D.Y. Murzin, Liquid phase hydrogenation of citral: suppression of side reactions, *Appl. Catal. A Gen.* 237 (2002) 181–200.
- [60] Y. Li, X. Xu, P. Zhang, Y. Gong, H. Li, Y. Wang, Highly selective Pd@mpg-C₃N₄ catalyst for phenol hydrogenation in aqueous phase, *RSC Adv.* 3 (2013) 10973–10982.
- [61] T. Kurita, F. Aoki, T. Mizumoto, T. Maejima, H. Esaki, T. Maegawa, Y. Monguchi, H. Sajiki, Facile and convenient method of deuterium gas generation using a Pd/C-catalyzed H₂-D₂ exchange reaction and its application to synthesis of deuterium-labeled compounds, *Chem. Eur. J.* 14 (2008) 3371–3379.
- [62] P. Beccat, J.-C. Bertolini, Y. Gauthier, J. Massardier, P. Ruiz, Crotonaldehyde and methylcrotonaldehyde hydrogenation over Pt(111) and Pt₈₀Fe₂₀(111) single crystals, *J. Catal.* 126 (1990) 451–456.